



Cite this: *RSC Adv.*, 2022, 12, 31317

# Vacancy defect engineered BiVO<sub>4</sub> with low-index surfaces for photocatalytic application: a first principles study†

Zhiyuan Zhang,‡ Yingchao Song,‡ Yuqi Xiang and Zhihong Zhu \*

BiVO<sub>4</sub> has been widely investigated as a photocatalyst material for water splitting due to its outstanding photocatalytic properties. In order to further improve its photocatalytic efficiency, it is necessary to conduct an in-depth study of improvement strategies, such as defect engineering. By focusing on the (001) and (011) surfaces, we carried out a systematic theoretical research on pristine and defective systems, including Bi, V and O vacancies. Based on density functional theory (DFT), the electronic properties, band alignments and Gibbs free energy of pristine and defective BiVO<sub>4</sub> have been analyzed. The electronic structures of the (001) and (011) surfaces show different band gaps, and O vacancies make the BiVO<sub>4</sub> become an n-type semiconductor, while Bi and V vacancies tend to form a p-type semiconductor. Moreover, the band edge positions indicate that holes are indeed easily accumulated on the (011) surface while electrons tend to accumulate on (001). However, the (011) surface with Bi and V vacancies does not have enough oxidation potential to oxidize water. The reaction free energy shows that O and Bi vacancies could lower the overpotential to some extent.

Received 5th August 2022  
Accepted 18th October 2022

DOI: 10.1039/d2ra04890f

rsc.li/rsc-advances

## 1. Introduction

Photocatalytic water splitting into H<sub>2</sub> or O<sub>2</sub> has received increasing attention because of its enormous potential to provide a green and renewable way to handle the energy crisis and solve environmental problems.<sup>1–3</sup> Since the discovery of the first photocatalyst a series of photocatalysts, such as Fe<sub>2</sub>O<sub>3</sub>, TiO<sub>2</sub>, WO<sub>3</sub>, SrTiO<sub>3</sub> and BiVO<sub>4</sub>, have been investigated for water splitting.<sup>4–8</sup> Among them, BiVO<sub>4</sub> has been identified as one of the most promising photocatalysts for water splitting due to its suitable band gap and nontoxic, low-cost and stable nature.<sup>9–12</sup> The valence band maximum (VBM) of individual BiVO<sub>4</sub> is well below the redox potential of water, causing an outstanding O<sub>2</sub> production ability, while its conduction band minimum (CBM) is less positive but very close to the H<sub>2</sub> evolution potential.<sup>13</sup> Moreover, BiVO<sub>4</sub> exhibits a large electron–hole separation yield because of the local polarization caused by the distortion of VO<sub>4</sub> tetrahedra.<sup>14</sup> However, the rapid recombination of carriers in

this photocatalyst results in a main bottleneck for photocatalytic efficiency, which limits the further application of BiVO<sub>4</sub> in this field.<sup>15</sup>

In order to further improve the photocatalytic efficiency of BiVO<sub>4</sub>, a series of methods have been researched, including morphology control, elemental doping, composite structure and defect engineering.<sup>16–21</sup> Recent research shows that defect formation can increase the charge separation efficiency and significantly improve the oxygen evolution reaction (OER) performance of BiVO<sub>4</sub> for water splitting.<sup>22–27</sup> The most common type of defect in BiVO<sub>4</sub> is oxygen vacancies, which can enhance the visible light absorption and promote the charge transfer. Therefore, the photocatalytic efficiency can be improved.<sup>28–30</sup> However, in some cases the oxygen vacancies might be counterproductive for photocatalytic performance by acting as electron–hole recombination centers.<sup>31</sup> Furthermore, when the Bi vacancy exists, a higher charge diffusion coefficient can be obtained. And the photocurrent density of this system increases remarkably, even higher than that of previously reported O vacancy engineered BiVO<sub>4</sub> under the same experimental conditions.<sup>32</sup> But defects are not always beneficial to improve the photocatalytic performance. V vacancy defect can induce additional states and act as the recombination centers, which cause the decrease of carrier lifetime and photocurrent.<sup>33</sup>

The modulation mechanism of defects has been extensively researched in recent years.<sup>34,35</sup> In BiVO<sub>4</sub>, the defects affect the electronic structure significantly and thereby the OER performance can be modulated.<sup>36</sup> However, their exact influence on OER is not fully understood due to studies are still limited and

College of Advanced Interdisciplinary Studies & Hunan Provincial Key Laboratory of Novel Nano Optoelectronic Information Materials and Devices, National University of Defense Technology, 410073 Changsha, Hunan, P. R. China. E-mail: zzhwcx@163.com

† Electronic supplementary information (ESI) available: Top view of optimized geometric structures of BiVO<sub>4</sub> surface. Free energy of H<sub>2</sub>, O<sub>2</sub> and H<sub>2</sub>O. Structures of the intermediates in the OER processes. Total energy and zero-point energy (ZPE) correction of adsorbates. Bader charge of pristine and defective BiVO<sub>4</sub>. See DOI: <https://doi.org/10.1039/d2ra04890f>

‡ These authors contributed equally to this work and should be considered co-first authors.



inconclusive.<sup>37,38</sup> Moreover, for a catalytic process, the reaction occurs on the surface of photocatalyst. Nevertheless most of researches are mainly concentrated on the electronic properties of bulk system with defects.<sup>37–40</sup> Therefore, it is necessary to conduct in-depth study of the defects under specific surface.

It has been confirmed that the BiVO<sub>4</sub> has the corner-cut truncated bipyramidal morphology. The (001) surface is the most stable,<sup>27,41–43</sup> while (011) and (101) comprise the majority of surface area. And the (001), (011), (101) comprise more than 99.3% of the surface area.<sup>44</sup> Moreover, (011) and (101) can be considered equivalent due to these two surfaces have similar surface energies and morphology.<sup>45</sup> Therefore, in this work, we focus on the (001) and (011) surfaces. The effect of O vacancy, Bi vacancy and V vacancy engineered BiVO<sub>4</sub> with representative surface have been investigated based on density functional theory (DFT). We focus on the electronic structure, band edge position and Gibbs free energy of pristine and defective BiVO<sub>4</sub>. The electronic structure of BiVO<sub>4</sub> has been investigated by calculating the partial density of states (DOS). The band edge positions are the focus of analyzing the photocatalytic mechanism. The photocatalytic activities of pristine and defective BiVO<sub>4</sub> are studied *via* analysis of the Gibbs free energy. Results show that Bi vacancy might be an effective mean with the lowest overpotential in our calculated systems. And the V vacancy could enhance the overpotential, thus it should be avoided in the experiment.

## 2. Computational details

All the structural optimization and static calculations are based on DFT, as implemented in the Vienna *ab initio* simulation package (VASP).<sup>46,47</sup> In the calculation, the projector-augmented wave (PAW) method is selected and the generalized gradient approximation (GGA) functional of Perdew, Burke and Ernzerhof (PBE) is used to describe exchange and correlation

potentials,<sup>48,49</sup> here the standard PAW potentials have been chosen. The 5d<sup>10</sup>6s<sup>2</sup>6p<sup>3</sup> of Bi, 3p<sup>6</sup>3d<sup>4</sup>4s<sup>1</sup> of V, and 2s<sup>2</sup>2p<sup>4</sup> of O are treated as the valence electrons. The convergence criterion for energy is 10<sup>−7</sup> eV for zero-point energy (ZPE) and 10<sup>−5</sup> for other calculations, 0.01 eV Å<sup>−1</sup> is selected for the convergence criterion of force. And a cut-off kinetic energy is set to 400 eV for plane wave functions. For BiVO<sub>4</sub> unit cell and surface system, the Monkhorst–Pack *k*-point grids setting are 7 × 7 × 5 and 4 × 4 × 1 to the first Brillouin zones, respectively. Also *U*<sub>3d</sub> = 2.7 eV has been used on V atom to correct the self-interaction error.<sup>11</sup> For the surface system, a vacuum region of 20 Å is added in order to avoid the interactions between layers. And the solvent effect has been considered for the Gibbs free energy calculations as implemented in VASPsol,<sup>50</sup> the water was selected as solvent here.

## 3. Results and discussion

### 3.1 Bulk geometric optimization

In our calculations, the unit cell of BiVO<sub>4</sub> has been optimized at first, and here the crystal cell and shape are allowed to be changed. Assuming *c* is the longest axis, the optimized lattice parameters are *a* = 5.17 Å, *b* = 5.16 Å, *c* = 11.76 Å, α = 89.999°, β = 90.003°, γ = 90.145°. The photocatalyst BiVO<sub>4</sub> exists in monoclinic scheelite (ms-) and tetragonal scheelite (ts-) phases. In the process of optimization based on DFT, the ms-BiVO<sub>4</sub> (*a* = 5.194 Å, *b* = 5.09 Å, *c* = 11.667 Å, α = β = 90°, γ = 90.4°) would spontaneously transform to ts-BiVO<sub>4</sub> (*a* = *b* = 5.147 Å, *c* = 11.722 Å, α = β = γ = 90°) when crystal cell and shape are allowed to be changed,<sup>41,51</sup> therefore, the BiVO<sub>4</sub> might tend to ts-BiVO<sub>4</sub> in our calculation, and the lattice constants slightly expand by less than 1% compared with ts-BiVO<sub>4</sub>. Due to ms-BiVO<sub>4</sub> and ts-BiVO<sub>4</sub> have a similar structure, both ms-BiVO<sub>4</sub> and ts-BiVO<sub>4</sub> can be used for calculating photocatalytic

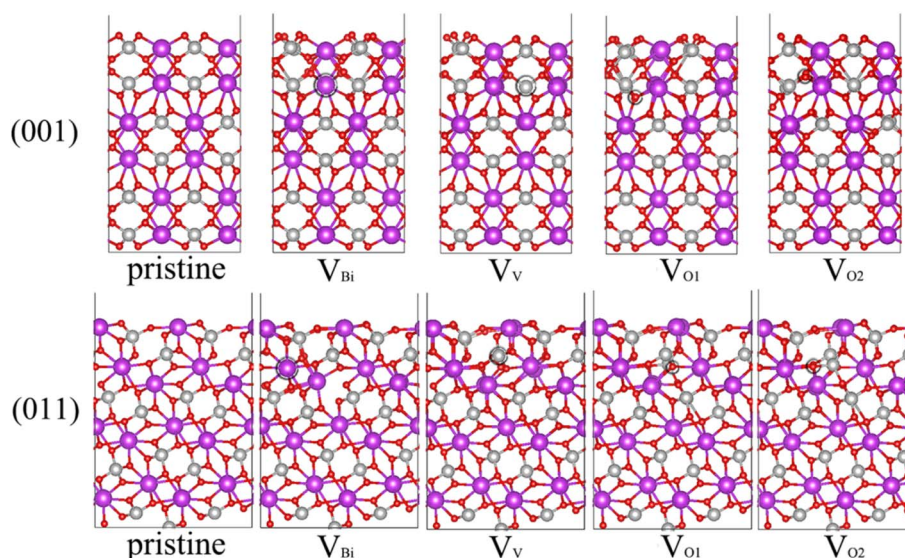


Fig. 1 Side view of optimized geometric structures of BiVO<sub>4</sub> surface. Bi (purple), V (silver) and O (red) atoms are shown in colored spheres. The vacancy site is marked by black circle.



performance, which would not change the important results and conclusions.<sup>52</sup>

### 3.2 Surface geometric structure

Due to the (001), (011) and (101) surfaces cover most area of  $\text{BiVO}_4$  and (011) and (101) can be considered equivalent,<sup>44,45</sup> thus we focus on (001) and (011) surfaces. In some previous studies, the  $b$  is set as the longest axis. In this case, the corresponding surfaces should define (010), (110) and (011). Moreover, there are some studies rotating the  $\text{BiVO}_4$  90° around the longest axis  $c$  compared our bulk  $\text{BiVO}_4$ , thus (011) should define (101) in these existent studies. For one  $\text{BiVO}_4$  unit cell, it contains one kind of Bi, one kind of V and two kinds of O.

Therefore, four possible kinds of vacancy defects of  $\text{BiVO}_4$  are examined, namely, Bi vacancy engineered  $\text{BiVO}_4$  ( $\text{V}_{\text{Bi}}$ ), V vacancy engineered  $\text{BiVO}_4$  ( $\text{V}_{\text{V}}$ ), the first kind of O vacancy engineered  $\text{BiVO}_4$  ( $\text{V}_{\text{O1}}$ ) and the second kind of O vacancy engineered  $\text{BiVO}_4$  ( $\text{V}_{\text{O2}}$ ), also the pristine  $\text{BiVO}_4$  with (001) and (011) surface are considered here. The unit cell of bulk  $\text{BiVO}_4$  has been cleaved to obtain the (001) and (011) surfaces, then the two slabs has been adjusted to make the thickness of them larger than 15 Å. And the  $\text{BiVO}_4$  (001) and (011) models are constructed by  $2 \times 2$  and  $2 \times 1$  corresponding slabs, respectively. The side and top views of optimized geometric structures are shown in Fig. 1 and S1,<sup>†</sup> respectively. The vacancy concentration of (001) is 4.2% for  $\text{V}_{\text{Bi}}$  and  $\text{V}_{\text{V}}$ , 1.0% for  $\text{V}_{\text{O1}}$  and  $\text{V}_{\text{O2}}$ , while that of (011) is 3.6% for  $\text{V}_{\text{Bi}}$ ,

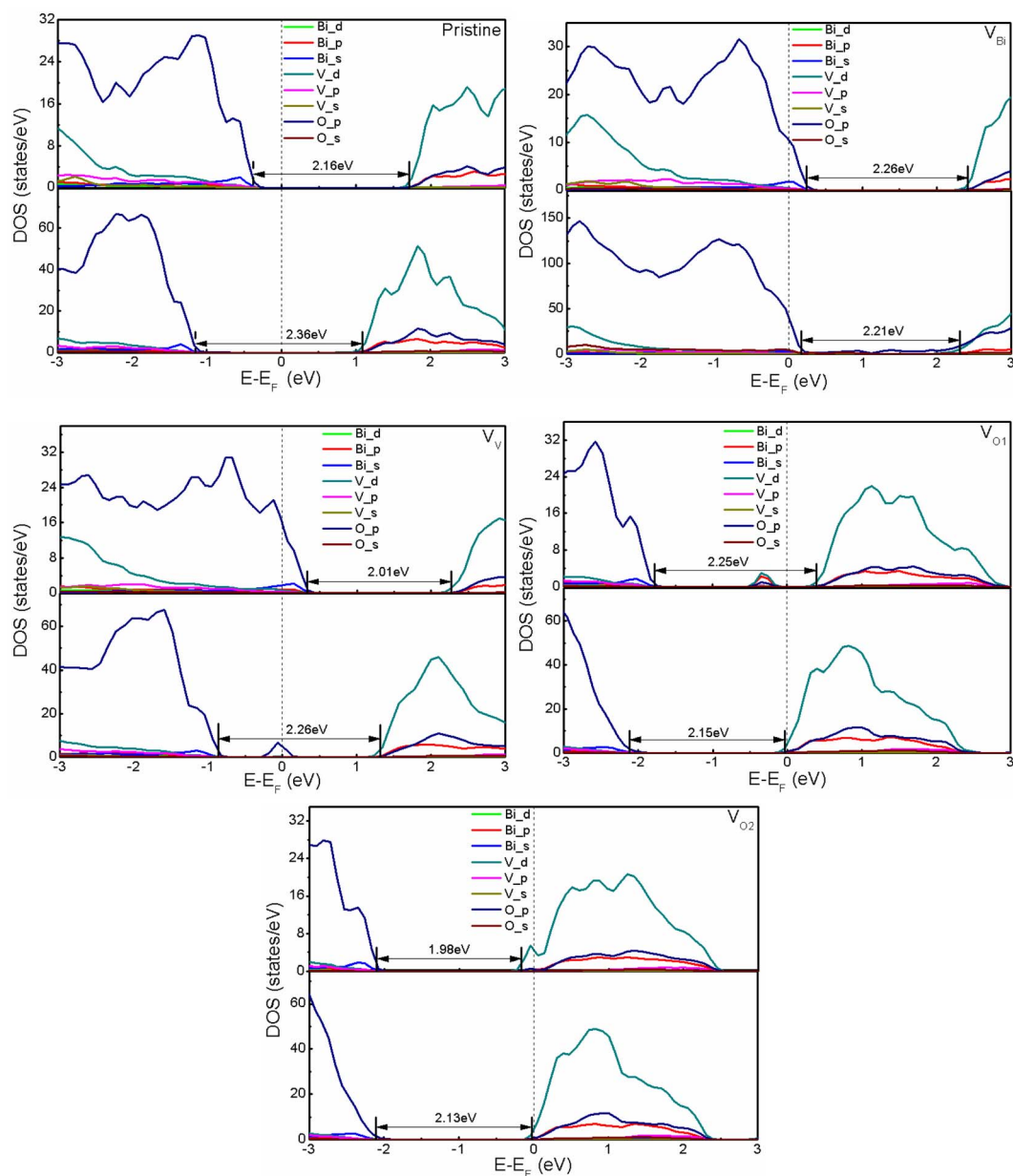


Fig. 2 The calculated DOS of pristine and defective  $\text{BiVO}_4$ . The upper part and bottom part represent (001) and (011), respectively. The Fermi level is set to zero.



3.3% for  $V_V$ , 0.9% for  $V_{O1}$  and  $V_{O2}$ . After carefully checking the structures of defective  $\text{BiVO}_4$ , it can be seen that the obvious distortion has been formed near the defect, which might modulate the electronic properties and affect the photocatalytic performance of  $\text{BiVO}_4$  significantly.

### 3.3 Electronic structures

After obtaining the most stable structures, the electronic structure of defective  $\text{BiVO}_4$  (001) and (011) have been investigated by calculating the partial DOS. And the calculated results are shown in Fig. 2. Clearly, the band gaps of pristine  $\text{BiVO}_4$  (001) and (011) are 2.16 eV and 2.36 eV, respectively. This result is consistent with the previous GGA +  $U$  calculation (2.123/2.083 eV for (001) surface and 2.244/2.250 eV for (011) surface)

and LDA +  $U$  calculation (2.18 eV for (001) surface and 2.38 eV for (011) surface).<sup>45,52</sup> And the Fermi level of pristine  $\text{BiVO}_4$  (001) is close to the VBM and far from the CBM, while that of pristine  $\text{BiVO}_4$  (011) is almost in the middle of band gap. Here the VBM is mainly populated by O 2p and the CBM is composed of V 3d in both pristine  $\text{BiVO}_4$  (001) and (011) systems. For the band edges of defective  $\text{BiVO}_4$  (001) and (011), also it can be observed VBM and CBM are contributed by O 2p and V 3d, respectively. However, there are still some differences existing in different structures, especially the Fermi level and band gap. It can be seen that  $V_{\text{Bi}}$  and  $V_V$  tend to make the pristine  $\text{BiVO}_4$  become a p-type semiconductor, while  $V_{O1}$  and  $V_{O2}$  tend to form a n-type semiconductor. Generically speaking, O vacancy is easy to form in the process of synthesis, thus the  $\text{BiVO}_4$  is often treated as

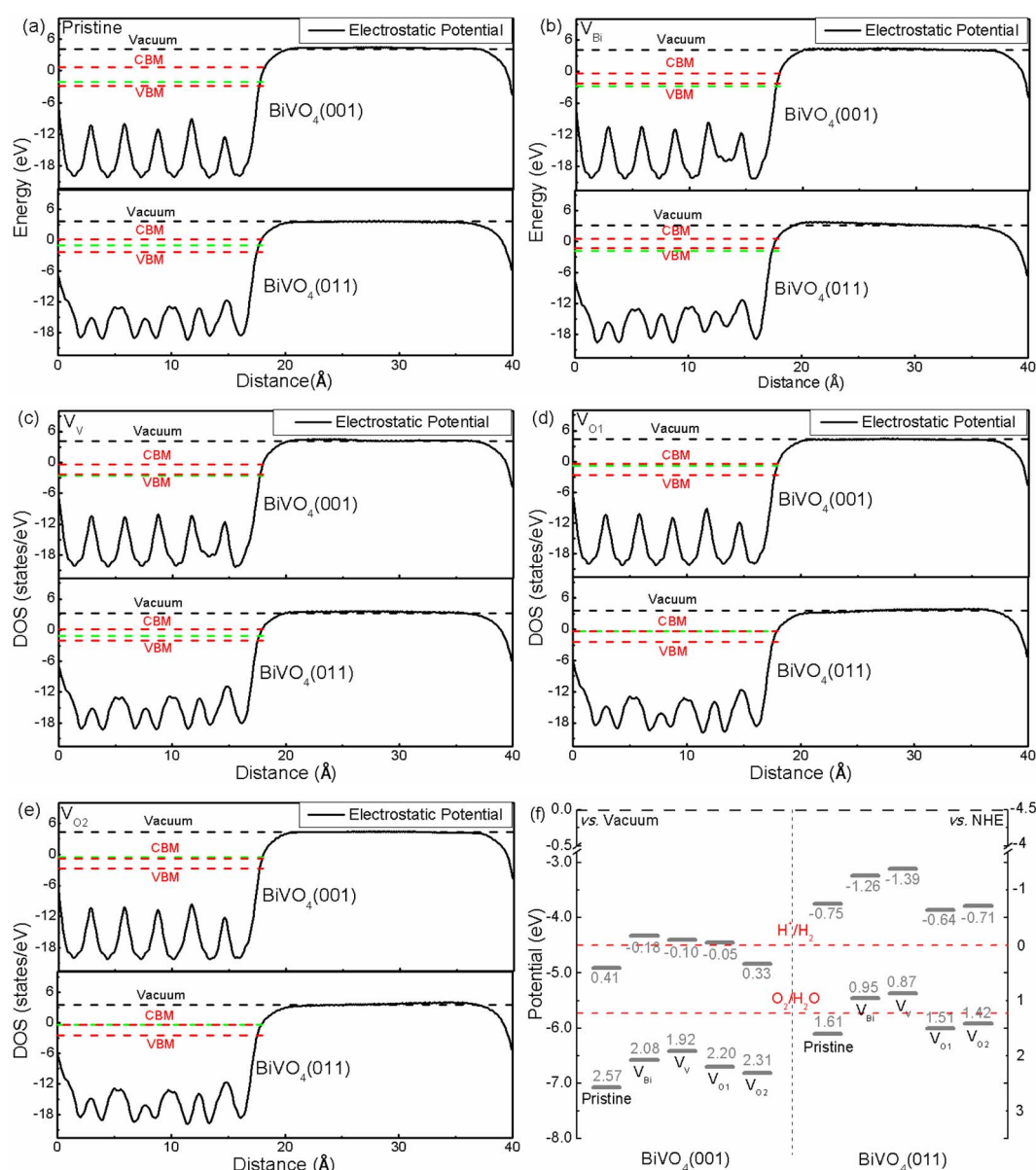


Fig. 3 (a)–(e) The relative positions of electrostatic potential of pristine and defective  $\text{BiVO}_4$ , (f) band edge potentials for  $\text{BiVO}_4$  (001) and (011). The green dash line represents the Fermi level.





a n-type semiconductor rather than p-type semiconductor in the experiments. This phenomenon indicates the  $V_{\text{Bi}}$  and  $V_{\text{V}}$  could introduce holes while  $V_{\text{O1}}$  and  $V_{\text{O2}}$  would introduce electrons, respectively. Moreover, the band gap, the Fermi level and band edge could be controlled by defects, indicating the oxidation and reduction capacity probably can be modulated according to introducing defects. Notably, a peak appears near the middle of band gap for  $V_{\text{V}}$  with (011) surface and  $V_{\text{O1}}$  with (001) surface. The peak of  $V_{\text{V}}$  with (011) is very close to the Fermi level, which might be caused by defect states, and it probably acts as the recombination center, which is not good for photocatalysis to some extent.

### 3.4 Band alignments

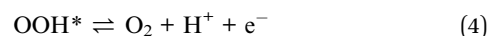
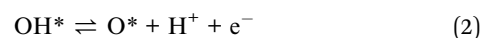
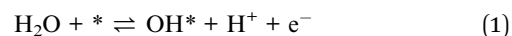
The band edge position is an important role for photocatalytic application. Hence the band edge position of  $\text{BiVO}_4$  has been analyzed based on macroscopic averaging method,<sup>53</sup> where the electrostatic potential has been chosen as a reference in order to obtain the band edge. The relative positions between the Fermi level and CBM/VBM are obtained according to their individual supercell. The results are shown in Fig. 3(a)–(e). Clearly, the electrostatic potentials of different facets are quite different. And the difference valued between CBM/VBM and vacuum level is 4.91/7.07 eV for pristine  $\text{BiVO}_4$  (001), and 3.75/6.11 eV for pristine  $\text{BiVO}_4$  (011), respectively, meaning the CBM and VBM of pristine  $\text{BiVO}_4$  (011) is higher than that of pristine  $\text{BiVO}_4$  (001). Therefore, the photogenerated electrons on the (011) would migrate to the (001) and the photogenerated holes could transfer from (001) to (011). This is consistent with the experimental results, where the researchers obtained direct evidence that holes are indeed easily accumulated on the (011) surface and electrons tend to accumulate on (001).<sup>54</sup> Although the average potentials of two facets are dramatically changed, similar behaviors could be found in  $V_{\text{Bi}}$ ,  $V_{\text{V}}$ ,  $V_{\text{O1}}$  and  $V_{\text{O2}}$ , where the CBM and VBM of (011) are still higher than that of (001). And the charge separation could be promoted near the crystal boundary of these two facets. Under the light irradiation, the photo-generated electrons would migrate to  $\text{BiVO}_4$  (001) from  $\text{BiVO}_4$  (011), and the photogenerated holes would transfer from  $\text{BiVO}_4$  (001) to  $\text{BiVO}_4$  (011) at the same time. Therefore, the  $\text{BiVO}_4$  (001) and  $\text{BiVO}_4$  (011) could be the reduction site and oxidation site, respectively. This result is consistent with the previous experimental results. Moreover, it can be inferred that the  $V_{\text{Bi}}$ ,  $V_{\text{V}}$ ,  $V_{\text{O1}}$  and  $V_{\text{O2}}$  cannot change this situation due to CBM and VBM of  $\text{BiVO}_4$  (011) are still higher than  $\text{BiVO}_4$  (001) after introducing these defects.

Considering the relationship between potentials of normal hydrogen electrode (NHE) and vacuum level ( $E_{\text{vacuum}} = -E_{\text{NHE}} - 4.5$  eV), the band edge positions related to  $\text{H}^+/\text{H}_2$  level and  $\text{O}_2/\text{H}_2\text{O}$  level are plotted, as shown in Fig. 3(f). We can see that the band edge positions are totally different. For (011) surface, the VBM of  $V_{\text{Bi}}$  and  $V_{\text{V}}$  are located above the corresponding  $\text{O}_2/\text{H}_2\text{O}$  potential, indicating the biased voltage is necessary for  $V_{\text{Bi}}$  and  $V_{\text{V}}$  to produce  $\text{O}_2$ . As for (001) surface, the VBM of pristine  $\text{BiVO}_4$ ,  $V_{\text{Bi}}$ ,  $V_{\text{V}}$ ,  $V_{\text{O1}}$  and  $V_{\text{O2}}$  are below the  $\text{O}_2/\text{H}_2\text{O}$  level, meaning these systems have ability to produce  $\text{O}_2$  without biased voltage.

Totally speaking, for (011) surface,  $V_{\text{Bi}}$  and  $V_{\text{V}}$  might not be a good way for photocatalytic application due to that the biased voltage must be added.

### 3.5 Overpotential

In order to further investigate the photocatalytic activity, the OER performance of pristine  $\text{BiVO}_4$ ,  $V_{\text{Bi}}$ ,  $V_{\text{V}}$ ,  $V_{\text{O1}}$  and  $V_{\text{O2}}$  with (001) and (011) surfaces have been analyzed according to overpotential. Here the computational hydrogen electrode (CHE) model has been adopted.<sup>55</sup> Generally speaking, there are four steps in the OER process, and each step contains one electron transfer. For the first step, the  $\text{H}_2\text{O}$  could be dissociated at the Bi site under the influence of photogenerated hole, and then a proton would be released and the OH radical would be formed. The second step is the reaction that OH radical releases another a proton and forms the O with the interaction of photogenerated hole. Then, the generated O would be combined with adjacent  $\text{H}_2\text{O}$ , forming the OOH radical and releasing a proton. At last, the OOH radical would further release a proton and form the  $\text{O}_2$ , then the  $\text{O}_2$  leaves the surface. The optimal OER reaction path could be described as:



where \* stands for the reaction site of photocatalyst, and  $\text{H}^*$ ,  $\text{OH}^*$ ,  $\text{O}^*$  and  $\text{OOH}^*$  refer to adsorbed intermediates in the OER process. The decisive role for overpotential ( $\eta$ ) is determined by the largest Gibbs free energy change ( $\Delta G$ ) among four reaction steps:

$$\eta = -\max[|\Delta G_{\text{OH}^*}|, |\Delta G_{\text{O}^*} - \Delta G_{\text{OH}^*}|, |\Delta G_{\text{OOH}^*} - \Delta G_{\text{O}^*}|, |4.92 - \Delta G_{\text{OOH}^*}|]/\text{e} - 1.23 \quad (5)$$

Without the biased voltage, the  $\Delta G$  can be obtained by calculating the difference of Gibbs free energy between product and reactant:

$$\Delta G = \Delta E + \Delta E_{\text{ZPE}} - T\Delta S \quad (6)$$

in which the  $\Delta E$  refers to adsorption energy,  $\Delta E_{\text{ZPE}}$  and  $\Delta S$  stand for ZPE and entropy at the specific temperature  $T$ , respectively. The relationship of Gibbs free energy in the CHE model meet the conditions:

$$G(\text{H}^+) + G(\text{e}^-) = 1/2G(\text{H}_2) \quad (7)$$

$$G(\text{H}^+) + G(\text{OH}^-) = G(\text{H}_2\text{O}) \quad (8)$$

$$2G(\text{H}_2) + G(\text{O}_2) - 2G(\text{H}_2\text{O}) = 4.92 \text{ eV} \quad (9)$$

In our calculation, the free energy of  $\text{O}_2$  is obtained by eqn (9) rather than DFT because of the large error for calculating  $\text{O}_2$  in



VASP program. The calculated free energy of  $\text{H}_2$ ,  $\text{O}_2$  and  $\text{H}_2\text{O}$  are listed in Table S1.†

After obtaining the free energy of  $\text{H}_2$ ,  $\text{O}_2$  and  $\text{H}_2\text{O}$ , the adsorbed intermediates have been investigated. The structures of adsorbed intermediates ( $\text{OH}^*$ ,  $\text{O}^*$  and  $\text{OOH}^*$ ) of pristine  $\text{BiVO}_4$ ,  $\text{V}_{\text{Bi}}$ ,  $\text{V}_{\text{V}}$ ,  $\text{V}_{\text{O1}}$  and  $\text{V}_{\text{O2}}$  with (001) and (011) surface are plotted in Fig. S2 and S3.† And the calculated total energy, ZPE and entropy for all the structures are shown in Table S2.† For these structures,  $\text{BiVO}_4$  substrate has been fixed and the adsorbed atom has been optimized at first, then the adsorbed atom and the top layer of substrate are relaxed together. The calculated results about overpotential of pristine and defective  $\text{BiVO}_4$  are shown in Fig. 4(a) and (b). For all the systems, the limiting step is the first step or the second step. Clearly,  $\text{V}_{\text{Bi}}$ ,  $\text{V}_{\text{V}}$ ,  $\text{V}_{\text{O1}}$  and  $\text{V}_{\text{O2}}$  could impact the free energy greatly. Here we focus on pristine  $\text{BiVO}_4$  at first. It can be found that (001) has a lower overpotential compared with (011). Hence, (011) is more active than (001) for OER. For this model, the overpotential is close to previous calculated studies, such as PBE0 with implicit solvent model calculation (1.2 V for (001) and 0.9 V for (011) surface) and GGA calculation (1.42 V for (001) and 1.14 V for (011) surface).<sup>44,56</sup> Then we turn to defective  $\text{BiVO}_4$ . For (001), it can be seen that the  $\text{V}_{\text{Bi}}$ ,  $\text{V}_{\text{V}}$ ,  $\text{V}_{\text{O1}}$  and  $\text{V}_{\text{O2}}$  could lower the free energy for forming  $\text{OH}^*$  and  $\text{OOH}^*$ . These two steps consist of one H removal, which is more efficient in all of the reaction steps happening on a surface. This phenomenon might be because the defects introduce additional holes or electrons near the Fermi level (the  $\text{V}_{\text{Bi}}$  and  $\text{V}_{\text{V}}$  introduce holes while  $\text{V}_{\text{O1}}$  and  $\text{V}_{\text{O2}}$  introduce electrons). These carriers could promote the charge transfer and lower the free energy. In the process of forming  $\text{O}^*$ ,  $\text{V}_{\text{Bi}}$ ,  $\text{V}_{\text{V}}$  show a lower free energy compared with pristine  $\text{BiVO}_4$ , while  $\text{V}_{\text{O1}}$  and  $\text{V}_{\text{O2}}$  show a higher free energy. This phenomenon might due to the pure O tend to be combined with holes rather than electrons for this surface, in these system, the  $\text{V}_{\text{Bi}}$ ,  $\text{V}_{\text{V}}$  introduce additional holes while  $\text{V}_{\text{O1}}$  and  $\text{V}_{\text{O2}}$  introduce electrons. Totally speaking, the  $\text{V}_{\text{O1}}$  and  $\text{V}_{\text{O2}}$  reduce the photocatalytic activity due to a large  $\Delta G$ , while  $\text{V}_{\text{V}}$  only lower the overpotential slightly and the difference could be negligible, thus  $\text{V}_{\text{V}}$  probably do not affect the photocatalytic performance for this surface. And  $\text{V}_{\text{Bi}}$  could improve the photocatalytic performance to some extent. Then we turn to OER on the (011)

surface, and here an analogous set of calculations was performed. The results show that the pristine (011) surface is the more efficient than (001), and the second step becomes the potential limiting step. With respect to the pristine surface, the free energy of defective  $\text{BiVO}_4$  with (011) surface show a different variation trend compared with (001). It can be seen that the  $\text{V}_{\text{O1}}$  and  $\text{V}_{\text{O2}}$  lower the free energy while  $\text{V}_{\text{Bi}}$  and  $\text{V}_{\text{V}}$  enhance the free energy for forming  $\text{OH}^*$ ,  $\text{O}^*$  and  $\text{OOH}^*$ . This phenomenon is completely different compared with (001), indicating the OH, O and OOH radicals might tend to be combined with electrons rather than holes for this surface. For (011) surface, we can see that the OER efficiency is reduced when the  $\text{V}_{\text{V}}$  is introduced, while it can be improved when the  $\text{V}_{\text{Bi}}$ ,  $\text{V}_{\text{O1}}$  and  $\text{V}_{\text{O2}}$  is introduced. The overpotential of  $\text{V}_{\text{O1}}$  and  $\text{V}_{\text{O2}}$  shows a similar behavior with some previous studies,<sup>57,58</sup> where the O vacancies enhance the overpotential for (001). However, there are also some previous studies showing a different situation, where the O vacancies lower the overpotential for (001) and enhance the overpotential for (011).<sup>44</sup> This phenomenon probably due to the different location of O vacancies, thus it can be inferred that O vacancies is an effective but uncontrollable method for OER. In our calculated systems, the  $\text{V}_{\text{V}}$  is not beneficial to enhance OER performance while  $\text{V}_{\text{Bi}}$  would contribute to improving OER performance. The calculated results is consistent with the previous experimental results.<sup>32,33</sup> Therefore, the  $\text{V}_{\text{V}}$  should be avoided in the experiment. And the  $\text{V}_{\text{Bi}}$  should be adopted to improve the OER performance.

### 3.6 Origins of free energy change

In order to reveal the origins of free energy change, the partial DOS of active sites and adsorbate have been examined. In a chemical reactions, the frontier molecular orbitals in the proximity of Fermi level play an important role.<sup>59</sup> As show in Fig. 5(a)–(f), it can be seen there are two or one hybridized states between active site and adsorbate for  $\text{O}^*$  and  $\text{OOH}^*$ . Totally speaking, two hybridized states near the Fermi level would have a lower free energy. For (001), the pristine  $\text{BiVO}_4$ ,  $\text{V}_{\text{Bi}}$  and  $\text{V}_{\text{V}}$  have a much lower free energy compared with  $\text{V}_{\text{O1}}$  and  $\text{V}_{\text{O2}}$  for  $\text{O}^*$ , and pristine  $\text{BiVO}_4$  has a much higher free energy compared with  $\text{V}_{\text{Bi}}$ ,  $\text{V}_{\text{V}}$ ,  $\text{V}_{\text{O1}}$  and  $\text{V}_{\text{O2}}$  for  $\text{OOH}^*$ . Moreover, the free energy would increase as the distance between two hybridized states

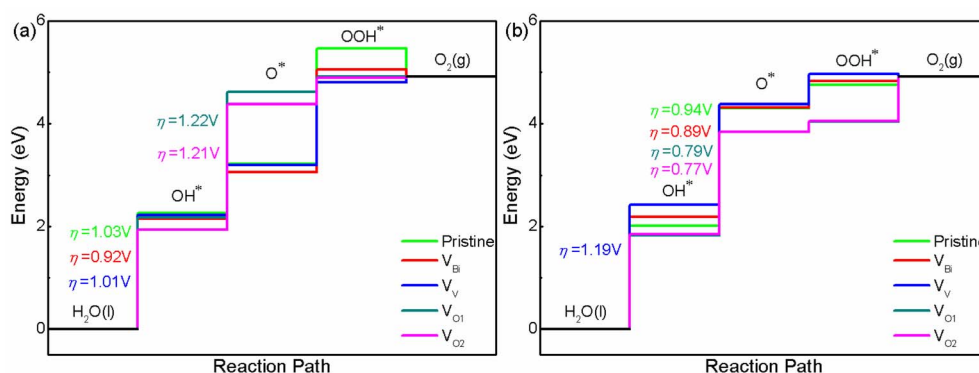


Fig. 4 The calculated OER free energy of (a)  $\text{BiVO}_4$  (001) and (b)  $\text{BiVO}_4$  (011).



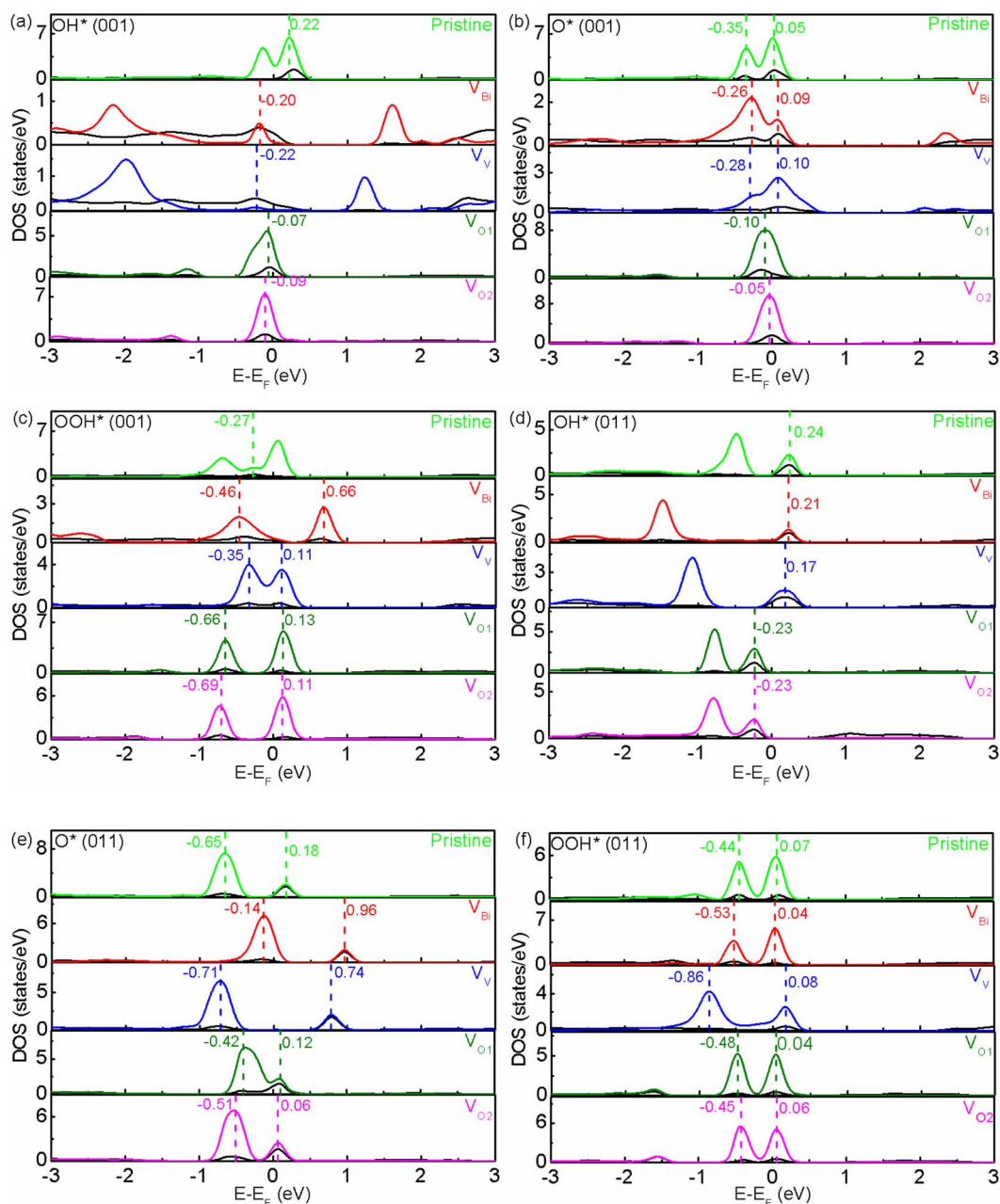


Fig. 5 (a)–(f) The partial DOS of pristine and defective  $\text{BiVO}_4$ . The black and multicoloured line represent the partial DOS of active site and adsorbate, respectively.

become greater. This phenomenon might due to a larger distance between two hybridized states increases the difficulty in transferring charge and weaken the adsorption. And one hybridized state makes the charge transfer more difficultly and further weaken the adsorption. Similar behavior also can be found in (011) although the exact locations of hybridized states are different. For  $\text{OH}^*$ , there is one hybridized state between active site and adsorbate. And it can be seen the free energy is lower when the hybridized state is below the Fermi level. Moreover, it can be found the free energy is related to the distance between the Fermi level and the hybridized state. When the hybridized state is below the Fermi level, the free

energy decrease with a smaller distance. However, when the hybridized state is above the Fermi level, the free energy is unexpectedly enhanced with a smaller distance. This result is difficult to explain and ought to be investigated in more detail in the future. We guess this phenomenon is due to positive charges have already accumulated on the active site, which would promote holes transfer and inhibit electrons transfer between active site and adsorbate. Therefore, the free energy could be modulated. The Bader charge analysis for active site has been shown in Fig. S4,<sup>†60</sup> it is clearly that positive charges have accumulated on the active site. After inducing defects, the charge distribution on this site has a slight, not obvious change.

According to the results of hybridized states and Bader charge, it can be inferred defects mainly affect the hybridized states between active site and adsorbate, thus the free energy for each step can be adjusted and the overpotential can be changed.

## 4. Conclusions

In summary, we have carried out a comprehensive periodic density functional theory (DFT) simulations for the defective BiVO<sub>4</sub> with (001) and (011) surfaces to improve its photocatalytic performance. It is found that defects have a great effect on BiVO<sub>4</sub>. V<sub>V</sub> with (011) surface and V<sub>O1</sub> with (001) surface create defect states near the middle of band gap, which might not be good for photocatalysis to some extent. The band edge position indicates that V<sub>Bi</sub> and V<sub>V</sub> with (011) cannot produce O<sub>2</sub> without biased voltage. According to modeling all of the reaction intermediates for different water oxidation mechanisms, we have shown that the most favorable photocatalytic process on BiVO<sub>4</sub> is the (011) surface. The defects could change the overpotential greatly, and V<sub>Bi</sub>, V<sub>O1</sub> and V<sub>O2</sub> exhibit the best photocatalytic activity due to its lower overpotential in our calculated systems. Moreover, the defects have a great effect on hybridized state between active site and adsorbate. By controlling the exposed surface facet and the vacancy content, OER performance can be improved, which is important for the design of novel photocatalyst.

## Conflicts of interest

There are no conflicts of interest to declare.

## Acknowledgements

Funding for this research was provided by National Natural Science Foundation of China (NSFC) (11674396).

## References

- 1 A. Fujishima and K. Honda, *Nature*, 1972, **238**, 37–38.
- 2 S. Anantharaj, S. R. Ede, K. Sakthikumar, K. Karthick, S. Mishra and S. Kundu, *ACS Catal.*, 2016, **6**, 8069–8097.
- 3 J. Eichhorn, C. Kastl, J. K. Cooper, D. Ziegler, A. M. Schwartzberg, I. D. Sharp and F. M. Toma, *Nat. Commun.*, 2018, **9**, 2597.
- 4 O. F. S. Khasawneh and P. Palaniandy, *Environ. Technol. Innovation*, 2021, **21**, 101230.
- 5 W. Zhang, H. He, H. Li, L. Duan, L. Zu, Y. Zhai, W. Li, L. Wang, H. Fu and D. Zhao, *Adv. Energy Mater.*, 2021, **11**, 2003003.
- 6 V. Dutta, S. Sharma, P. Raizada, V. K. Thakur, A. A. P. Khan, V. Saini, A. M. Asiri and P. Singh, *J. Environ. Chem. Eng.*, 2021, **9**, 105018.
- 7 S. Patial, V. Hasija, P. Raizada, P. Singh, A. A. P. K. Singh and A. M. Asiri, *J. Environ. Chem. Eng.*, 2020, **8**, 103791.
- 8 H. L. Tan, R. Amal and Y. H. Ng, *J. Mater. Chem. A*, 2017, **5**, 16498–16521.
- 9 S. C. Wang, P. Chen, Y. Bai, J. H. Yun, G. Liu and L. Z. Wang, *Adv. Mater.*, 2018, **30**, 1800486.
- 10 Y. C. Qiu, W. Liu, W. Chen, G. M. Zhou, P. C. Hsu, R. F. Zhang, Z. Liang, S. S. Fan, Y. G. Zhang and Y. Cui, *Sci. Adv.*, 2016, **2**, 1501764.
- 11 T. W. Kim, Y. Ping, G. A. Galli and K. S. Choi, *Nat. Commun.*, 2015, **6**, 8769.
- 12 L. Zhou, C. Q. Zhao, B. Giri, P. Allen, X. W. Xu, H. Joshi, Y. Y. Fan, L. V. Titova and P. M. Rao, *Nano Lett.*, 2016, **16**, 3463–3474.
- 13 C.-K. Huang, T. Wu, C.-W. Huang, C.-Y. Lai, M.-Y. Wu and Y.-W. Lin, *Appl. Surf. Sci.*, 2017, **399**, 10–19.
- 14 Z. Zhao, Z. Li and Z. Zou, *Phys. Chem. Chem. Phys.*, 2011, **13**, 4746–4753.
- 15 Y. Chen, T. Shi, P. Liu, X. Ma, L. Shui and C. Shang, *J. Mater. Chem. A*, 2018, **6**, 19167–19175.
- 16 M. Huang, C. Li, L. Zhang, Q. Chen, Z. Zhen, Z. Li and H. Zhu, *Adv. Energy Mater.*, 2018, **8**, 1802198.
- 17 J. Wang, L. Xu, T. Wang, R. Li, Y. Zhang, J. Zhang and T. Peng, *Adv. Energy Mater.*, 2021, **11**, 2003575.
- 18 J. Safaei, H. Ullah, N. A. Mohamed, M. F. M. Noh, M. F. Soh and A. A. Tahir, *Appl. Catal., B*, 2018, **234**, 296–310.
- 19 T. W. Kim and K. S. Choi, *Science*, 2014, **343**, 990–994.
- 20 J. Mao, Z. Gu, Y. Yu, H. Liu, J. Qu and X. An, *ACS Appl. Energy Mater.*, 2021, **4**, 2543–2551.
- 21 R. Guo, A. Yan, J. Xu, B. Xu, T. Li, X. Liu, T. Yi and S. Luo, *J. Alloys Compd.*, 2020, **817**, 153246–153257.
- 22 X. Lu, K. Ye, S. Zhang, J. Zhang, J. Yang, Y. Huang and H. Ji, *Chem. Eng. J.*, 2022, **428**, 131027.
- 23 M. A. Gaikwad, U. P. Suryawanshi, U. V. Ghorpade, J. S. Jang, M. P. Suryawanshi and J. H. Kim, *Small*, 2022, **18**, 2105084.
- 24 S. Liu, R. Gao, R. Zhang, Z. Wang, X. Liu, T. Nakajima, X. Zhang, Y. Su and L. Wang, *Appl. Catal., B*, 2021, **298**, 120610.
- 25 Z. Kang, X. Lv, Z. Sun, S. Wang, Y. Zheng and X. Tao, *Chem. Eng. J.*, 2021, **421**, 129819.
- 26 M. Lamers, S. Fiechter, D. Friedrich, F. F. Abdi and R. Krol, *J. Mater. Chem. A*, 2018, **6**, 18694–18700.
- 27 S. M. Thalluri, S. Hernández, S. Bensaida, G. Saracco and N. Russo, *Appl. Catal., B*, 2016, **180**, 630–636.
- 28 S. Wang, P. Chen, Y. Bai, J. Yun, G. Liu and L. Wang, *Adv. Mater.*, 2018, **30**, 1800486.
- 29 X. Zhao, J. Hu, X. Yao, S. Chen and Z. Chen, *ACS Appl. Energy Mater.*, 2018, **1**, 3410–3419.
- 30 B. Zhang, L. Wang, Y. Zhang, Y. Ding and Y. Bi, *Angew. Chem., Int. Ed.*, 2018, **57**, 2248–2252.
- 31 S. Wang, T. He, P. Chen, A. Du, K. Ostrikov, W. Huang and L. Wang, *Adv. Mater.*, 2020, **32**, 2001385.
- 32 Y. Lu, Y. Yang, X. Fan, Y. Li, D. Zhou, B. Cai, L. Wang, K. Fan and K. Zhang, *Adv. Mater.*, 2022, **34**, 2108178.
- 33 T. Tran-Phu, Z. Fusco, I. D. Bernardo, J. Lipton-Duffin, C. Y. Toe, R. Daiyan, T. Gengenbach, C. Lin, R. Bo, H. T. Nguyen, G. M. J. Barca, T. Wu, H. Chen, R. Amal and A. Tricoli, *Chem. Mater.*, 2021, **33**, 3553–3565.
- 34 S. Lardhi, L. Cavallo and M. Harb, *J. Phys. Chem. C*, 2018, **122**, 18204–18211.





- 35 N. Österbacka, F. Ambrosio and J. Wiktor, *J. Phys. Chem. C*, 2022, **126**, 2960–2970.
- 36 W. Yin, S. Wei, M. M. Al-Jassim, J. Turner and Y. Yan, *Phys. Rev. B: Condens. Matter Mater. Phys.*, 2011, **83**, 155102.
- 37 H. Ullah, A. A. Tahir and T. K. Mallick, *Appl. Catal., B*, 2018, **224**, 895–903.
- 38 M. D. Bhatt and J. Y. Lee, *J. Electroanal. Chem.*, 2018, **828**, 97–101.
- 39 T. Liu, M. Cui and M. Dupuis, *J. Phys. Chem. C*, 2020, **124**, 23038–23044.
- 40 J. Zhang, X. Chen, M. Deng, H. Shen, H. Li and J. Ding, *Phys. Chem. Chem. Phys.*, 2020, **22**, 25297–25305.
- 41 N. Österbacka and J. Wiktor, *J. Phys. Chem. C*, 2021, **125**, 1200–1207.
- 42 D. Wang, H. Jiang, X. Zong, Q. Xu, Y. Ma, G. Li and C. Li, *Chem.–Eur. J.*, 2011, **17**, 1275–1282.
- 43 J. Yang, D. Wang, X. Zhou and C. Li, *Chem.–Eur. J.*, 2013, **19**, 1320–1326.
- 44 P. Nikačević, F. S. Hegner, J. R. Galán-Mascarós and N. López, *ACS Catal.*, 2021, **11**, 13416–13422.
- 45 J. Hu, W. Chen, X. Zhao, H. Su and Z. Chen, *ACS Appl. Mater. Interfaces*, 2018, **10**, 5475–5484.
- 46 G. Kresse and J. Furthmüller, *Phys. Rev. B: Condens. Matter Mater. Phys.*, 1996, **54**, 11169–11186.
- 47 G. Kresse and J. Furthmüller, *Comput. Mater. Sci.*, 1996, **6**, 15–50.
- 48 P. Geerlings, F. De Proft and W. Langenaeker, *Chem. Rev.*, 2003, **103**, 1793–1873.
- 49 P. Perdew, K. Burke and M. Ernzerhof, *Phys. Rev. Lett.*, 1996, **77**, 3865–3868.
- 50 K. Mathew, R. Sundararaman, K. Letchworth-Weaver, T. A. Arias and R. G. Hennig, *J. Chem. Phys.*, 2014, **140**, 084106.
- 51 I. Laraib, M. A. Carneiro and A. Janotti, *J. Phys. Chem. C*, 2019, **123**, 26752–26757.
- 52 J. Shi, W. Zhang and Q. Gu, *J. Phys. Chem. C*, 2022, **126**, 9541–9550.
- 53 C. G. Van de Walle and R. M. Martin, *Phys. Rev. B: Condens. Matter Mater. Phys.*, 1986, **34**, 5621.
- 54 Y. Zhao, R. Li, L. Mu and C. Li, *Cryst. Growth Des.*, 2017, **17**, 2923–2928.
- 55 J. K. Nørskov, J. Rossmeisl, A. Logadottir, L. Lindqvist, J. R. Kitchin, T. Bligaard and H. Jonsson, *J. Phys. Chem. B*, 2004, **108**, 17886–17892.
- 56 P. Li, X. Chen, H. He, X. Zhou, Y. Zhou and Z. Zou, *Adv. Mater.*, 2018, **30**, 1703119.
- 57 A. Massaro, A. Pecoraro, S. Hernandez, G. Talarico, A. B. Munoz-García and M. Pavone, *Mol. Catal.*, 2022, **517**, 112036.
- 58 J. Hu, X. Zhao, W. Chen, H. Su and Z. Chen, *J. Phys. Chem. C*, 2017, **121**, 18702–18709.
- 59 K. Fukui, *Science*, 1982, **218**, 747–754.
- 60 G. Henkelman, A. Arnaldsson and H. Jónsson, *Comput. Mater. Sci.*, 2006, **36**, 354.

